frontiers in
NEUROENERGETICS

ORIGINAL RESEARCH ARTICLE
published: 18 November 2009
doi: 10.3389/neuro.14.007.2009

The possible role of CO_2 in producing a post-stimulus CBF and BOLD undershoot

Meryem A. Yücel*[1,2], *Anna Devor*[2,3], *Ata Akın*[1] and *David A. Boas*[2]

[1] *Institute of Biomedical Engineering, Boğaziçi University, Istanbul, Turkey*
[2] *HMS/MIT/MGH Athinoula A. Martinos Center for Biomedical Imaging, Charlestown, MA, USA*
[3] *Department of Neurosciences, University of California San Diego, La Jolla, CA, USA*

Edited by:
Bruno Weber, University of Zurich, Switzerland

Reviewed by:
Kamil Uludağ, Max Planck Institute, Germany
Fahmeed Hyder, Yale University, USA

****Correspondence:***
David A. Boas, Harvard Medical School, 13th Street Building 149, Charlestown, MA 02129, USA.
e-mail: dboas@nmr.mgh.harvard.edu

Comprehending the underlying mechanisms of neurovascular coupling is important for understanding the pathogenesis of neurodegenerative diseases related to uncoupling. Moreover, it elucidates the casual relation between the neural signaling and the hemodynamic responses measured with various imaging modalities such as functional magnetic resonance imaging (fMRI). There are mainly two hypotheses concerning this mechanism: a metabolic hypothesis and a neurogenic hypothesis. We have modified recent models of neurovascular coupling adding the effects of both NO (nitric oxide) kinetics, which is a well-known neurogenic vasodilator, and CO_2 kinetics as a metabolic vasodilator. We have also added the Hodgkin–Huxley equations relating the membrane potentials to sodium influx through the membrane. Our results show that the dominant factor in the hemodynamic response is NO, however CO_2 is important in producing a brief post-stimulus undershoot in the blood flow response that in turn modifies the fMRI blood oxygenation level-dependent post-stimulus undershoot. Our results suggest that increased cerebral blood flow during stimulation causes CO_2 washout which then results in a post-stimulus hypocapnia induced vasoconstrictive effect.

Keywords: carbon dioxide, nitric oxide, cerebral blood flow, vasodilation, $CMRO_2$, fMRI

INTRODUCTION

In order to meet the expected increased demand of the brain for glucose and oxygen during neuronal activation, the activated area stimulates vasodilation which leads to an increase in local cerebral blood flow (CBF) and cerebral blood volume (CBV), and hence an increased delivery of glucose and oxygen (Iadecola and Nedergaard, 2007; Irani et al., 2007; Metea and Newman, 2007). While neurons and astrocytes produce the signals of vasodilation, endothelial cells, pericytes and smooth muscle cells transduce these signals into a change in CBF in a healthy brain (Girouard and Iadecola, 2006; Drake and Iadecola, 2007; Schummers et al., 2008). This phenomenon is called neurovascular coupling. This coupling is tightly controlled via numerous biological signaling pathways. The control may be via metabolic factors (CO_2, K^+, adenosine etc.) or via neurogenic factors (neurotransmitters, NO etc.) (Estrada and DeFelipe, 1998).

Maintaining this synchronous control is vital, since any impairment in it may lead to ischemic lesions and even toxicity due to excess of metabolic factors (Girouard and Iadecola, 2006). The dissynchrony may also occur under many pathological conditions such as Alzheimer disease, hypertension, ischemic stroke (Girouard and Iadecola, 2006), migraine (Akın et al., 2006) and Huntington's disease (Clark et al., 2002). Importantly, understanding details of normal coupling and its disruption in disease will guide identification of possible treatment options.

In spite of the knowledge of many vasodilators, such as nitric oxide, arachidonic acid, potassium (K^+), CO_2, bicarbonate and adenosine, their relationship to neurovascular coupling is not fully understood. Among them, the vasodilatory role of nitric oxide during neuronal activity has been shown both during flicker stimuli in cat optic nerve (Buerk et al., 1996) and during forepaw stimuli in rat somatosensory areas (Buerk et al., 2003). There are mainly two hypotheses that are used to explain brain hemodynamics in terms of these vasodilators (Estrada and DeFelipe, 1998; Riera et al., 2008). According to the first hypothesis, namely the metabolic hypothesis, local CBF increase is a result of several vasodilators such as CO_2, K^+ and adenosine which are the metabolic products of neuronal activation (Estrada and DeFelipe, 1998). Whereas according to the second hypothesis, the neurogenic hypothesis, local CBF is maintained via vasodilator neurotransmitters that are 'synaptic products' released by the neurons as a result of neuronal activation (Estrada and DeFelipe, 1998; Riera et al., 2008). However, recent studies have shown that the coexistence of both neurogenic and metabolic factors is needed to regulate cerebral perfusion (Ito et al., 2005; Riera et al., 2008). In this study we aim to compare the relative importance of these two neurovascular coupling hypotheses in producing changes in CBF, blood volume, and oxygenation.

Brain hemodynamics is intensely studied using different neuroimaging modalities such as functional magnetic resonance imaging (fMRI), positron emission tomography (PET) and optical imaging. Each one of these modalities provides valuable insight into specific components of neurovascular coupling. Recent work in neuroimaging studies demonstrates that not only integration of multiple neuroimaging modalities is required, but that mathematical modeling is necessary to understand the complex physiology underlying neurovascular coupling. There are numerous models aiming to explain either the vascular or the

neurometabolic response to brain activation. The Balloon and Windkessel models are among the ones describing the vascular response. According to the Balloon model, the venous compartment expands as a result of the output of the capillary bed (Buxton et al., 1998). The Windkessel model extends the balloon model to incorporate vascular compliance (Mandeville et al., 1999). A neurometabolic model that couples brain electrical activity and energy metabolism via the Na^+–K^+ pump and mitochondrial respiration was developed by Aubert and Costalat (2002). They recently extended that model by adding an astrocytic compartment (Aubert and Costalat, 2005). There exist models that combine the vascular and metabolic compartments to investigate how CBF is controlled via metabolic and neurogenic pathways. Banaji's model is a good example that focuses on autoregulation of the blood vessels via different feedback mechanisms (Banaji et al., 2005). While these are just a few of the numerous models described in the literature, in general there is a need for a model which describes CBF in terms of both neurogenic and metabolic mediators that are directly related to the neuronal stimulus as an input to the model.

We have constructed a biochemical model of neurovascular coupling which has the action potential firing frequency as an input. We have set CBF dependent on the neuronal signals resulting from synaptic activity, NO, and as a result of an energy metabolism product, CO_2. We have chosen NO among the other vasodilators, since it has been shown by many studies that NO related increases in CBF is more dominant compared with other vasodilators at specific brain regions such as cerebellum (Yang et al., 1999, 2003) and somatosensory cortex (Lindauer et al., 1999). Our choice of CO_2, which is a product of oxidative phosphorylation, is based on the fact that increases in CO_2 decreases the pH of the medium (Chen and Anderson, 1997), leading to a significant increase in CBF (Kety and Schmidt, 1948). The model input is the frequency of the action potentials generated by the neurons in response to a stimulus, and CBF, blood oxygenation level-dependent (BOLD) signal, CBV and the metabolite concentrations are the outputs of the system. This input triggers both the energy pathways and synaptic activity. We have first tested the relative contributions of neurogenic and metabolic pathways for evoking changes in the CBF, BOLD and partial pressure of CO_2 (pCO_2) and interpret our findings in the context of existing experimental findings described in the literature (Hoge et al., 1999a,b; Kim et al., 1999; Uludağ et al., 2004; Wise et al., 2007), paying attention to differences that arise as stimulus duration increases from tens of seconds to a couple of minutes.

MATERIALS AND METHODS

MODEL DESCRIPTION

Our model is designed to explore the relative importance of two neurovascular coupling mechanisms in producing a blood flow response given changes in the frequency of action potentials: one of metabolic origin and the other neurogenic. The metabolic mechanism is based on the product of oxidative phosphorylation, carbon dioxide; whereas the neurogenic mechanism is based on nitric oxide, a synaptic activity product (**Figure 1**). These two factors diffuse to the extracellular matrix and then to blood vessels and produce vasodilation in the arterioles giving rise to changes in regional CBF and the BOLD signal.

The model has one input which is the frequency of action potentials. This can be kept constant or can be expressed as a time-dependent function throughout the stimulus duration. This frequency modulates the cell membrane potential by changing the flux of sodium and calcium ions across the membrane resulting in energy-product related and synaptic activity related vasodilation respectively. The sodium entry into the cell during an action potential increases the intra-cellular sodium concentration, thus increasing the Na^+–K^+ pump rate and consumption of adenosine triphosphate (ATP). The ATP supply for Na^+–K^+ pump comes from the phosphocreatine buffer, glycolysis, and mitochondrial respiration. Glucose (GLC) is delivered to the tissue by the vessels, and it turns into pyruvate (PYR) by passing through the glycolysis intermediary steps: glyceraldehyde-3-phosphate (GAP) and phosphoenolpyruvate (PEP). After this point PYR either goes to mitochondria and starts oxidative phosphorylation via aerobic respiration, or it turns into lactate (LAC) via anaerobic respiration. During these processes, there is a continuous electron transfer between nicotinamide adenine dinucleotide (NAD) and reduced nicotinamide adenine dinucleotide (NADH), and a phosphate transfer between ATP and adenosine diphosphate (ADP).

The equations describing sodium membrane transport, the Na^+–K^+ pump, neuronal energy metabolism (phosphocreatine buffer, glycolysis), and blood-brain-barrier exchange reactions are provided by Aubert and Costalat (2002), and the equations for NADH kinetics and mitochondrial respiration are provided by Aubert et al., (2007). The vasodilator carbon dioxide is produced as a result of oxidative phosphorylation. The other vasodilator nitric oxide, NO, is produced as a result of calcium (Ca^{2+}) entry into the neuron which activates NO production. NO then diffuses to and enters the smooth muscle cells around the arterioles. It then inhibits Ca^{2+} efflux from internal Ca^{2+} sources in these cells and so leads to vasodilation (Toda and Okamura, 1998). CBF is assumed to be dependent only on arteriolar diameter changes as given by Poiseuille's equation, and the pressure drop between the two ends of the vessel is assumed to be constant. The BOLD signal is then derived from $CMRO_2$ and CBF using Davis' BOLD equation (Davis et al., 1998).

In the next subsections, we provide details of each step in our model. The initial conditions for the new variables added to Aubert's model in this work are presented in **Table 1**, and all parameters are defined in **Table 2**. Unless otherwise stated, concentrations of metabolites are in mmol/L. The reaction rates are in mmol/L s. The subscripts within the tables and the text are a, arteriole; n, neuron; v, venule; c, capillary (in our case capillary stands for pre-capillary arteriole); sm, smooth muscle.

ACTION POTENTIALS MODULATE INTRA-CELLULAR NA^+ AND CA^{2+} CONCENTRATIONS

Our model uses action potential frequency as an input. In our model, the action potential frequency is assumed to be almost 0 before and after the stimulus and taken as 150 Hz during the

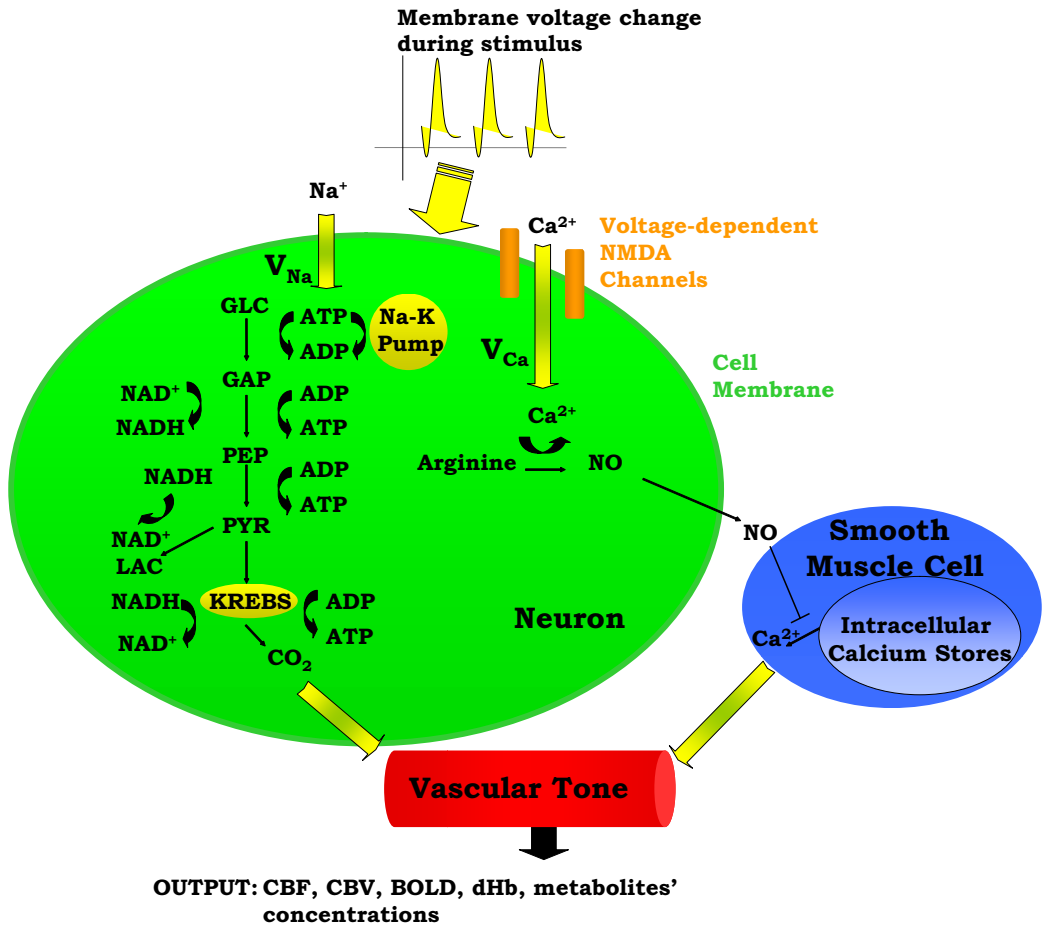

FIGURE 1 | A Schematic representation of the proposed model. ADP, adenosine diphosphate; AP, action potential; ATP, adenosine triphosphate; BOLD, blood oxygenation level-dependent; Ca^{2+}, calcium; CBF, cerebral blood flow; CBV, cerebral blood volume; CO_2, carbon dioxide; dHb, deoxyhemoglobin; GAP, glyceraldehyde-3-phosphate; GLC, glucose; K, potassium; LAC, lactate; Na, sodium; NAD^+, nicotinamide adenine dinucleotide; NADH, reduced nicotinamide adenine dinucleotide; NO, nitric oxide; PEP, phosphoenolpyruvate; PYR, pyruvate.

Table 1 | Initial values for the variables of the model.

Intracellular carbon dioxide (CO_{2n})	1.25 mM
Capillary carbon dioxide (CO_{2c})	1.23 mM
Intracellular calcium (Ca_n^{2+})	6937 nM
Intracellular nitric oxide (NO_{sm})	0.18 nM
Neuronal nitric oxide (NO_n)	0.21 nM

The concentrations above are obtained via equating Eqs. 4 and 6 to zero for CO_{2n} and CO_{2c}, Eq. 8 for Ca_n^{2+} and Eqs. 10 and 14 for NO_n and NO_{sm} (see Materials and Methods for the equations).

stimulus. We have fit a gaussian function to a generic action potential (Bean, 2007) to obtain the membrane voltage changes as a function of time,

$$\tilde{V}(t) = a_1 \times \exp\left(-\left(\frac{t-b_1}{c_1}\right)^2\right) + a_2 \times \exp\left(-\left(\frac{t-b_2}{c_2}\right)^2\right) \quad (1)$$

$$+ a_3 \times \exp\left(-\left(\frac{t-b_3}{c_3}\right)^2\right) + a_4 \times \exp\left(-\left(\frac{t-b_4}{c_4}\right)^2\right)$$
$$+ a_5 \times \exp\left(-\left(\frac{t-b_5}{c_5}\right)^2\right),$$

Where $\tilde{V}(t)$ is the voltage in mV as a function of time t and the remaining parameters are specified in **Table 2**. The voltage change for a train of action potentials is obtained by convolving Eq. 1 with the sequence of action potentials $[S(t)]$ as:

$$V(t) = \int_0^\infty \tilde{V}(t')S(t-t')\mathrm{d}t, \quad (2)$$

where $S(t)$ is equal to 0 unless t is at the onset of an action potential such that $S(t) = \sum_n \delta(t - t_n)$. For example, for action potentials arriving at a frequency of 100 Hz, $t_n = n\,\Delta t$ where $\Delta t = 10$ ms.

Table 2 | Parameters for the rate equations.

Equation	Constants	Description	Reference
1	$a_1 = 34.83$ $b_1 = 0.0001904$ $c_1 = 0.001559$ $a_2 = 37.97$ $b_2 = 0.002051$ $c_2 = 0.0002703$ $a_3 = 40.96$ $b_3 = 0.002259$ $c_3 = 0.0001748$ $a_4 = 75.48$ $b_4 = 0.001903$ $c_4 = 0.0005914$ $a_5 = -9.597e + 015$ $b_5 = -0.7747$ $c_5 = 0.1367$	Fitting constants for a single action potential	
4	$n_{Aero} = 3$	Stoichiometric constant	Aubert and Costalat (2002)
5a,b	$D_{new,CO_2} = 1.31 s^{-1}$	Diffusion rate for CO_2	See text for calculation
5b	$D_{CO_2} = 1.6 \times 10^{-5}$ cm^2/s	Diffusion constant for CO_2	Gros and Moll (1971)
5b	$d_{eff} = 35$ μm	Effective diffusion distance for CO_2	The same value as for NO (see below)
7	$CO_{2a} = 0.635$ mM	CO_2 concentration in arteriole	Lumb (2003)
9	$\tau_{Ca^{2+}} = 0.780$ s	Decay constant for calcium	Majewska et al. (2000)
12a,b	$D_{new,\,NO} = 3.3\ s^{-1}$	Diffusion rate for NO	See text for calculation
12b	$D_{NO} = 4 \times 10^{-5}$ cm^2/s	Diffusion constant for NO	Seraya and Nartsissov (2002), Kavdia and Popel (2004)
12b	$d_{eff} = 35$ μm	Effective diffusion distance for NO	Vaughn et al. (1998)
13, 15	$\tau_{NO} = 0.5$ s	Decay constant for NO	Vaughn et al. (1998) (0.1–1 s^{-1})
17b	$\alpha_{CO_2} = 0.0308$ mmolL^{-1} mmHg^{-1}	Solubility constant for CO_2	Lumb (2003)
18b	$Ca^{2+}_{sm,max} = 3563$ nM	Maximum Ca^{2+} concentration in smooth muscle	Range in Wada et al. (1999)
20a	$\Delta P = 266.6$ kg/ms^2	Pressure difference between the two ends of a precapillary arteriole	Cabrales et al. (2005)
20a	μ = 0.001 kg/ms (0% Hct) = 0.01 kg/ms (45% Hct)	Viscosity	Freitas (1999)
20b	$L = 1.8$ mm	Length of a precapillary arteriole	BME Handbook
21	$\alpha = 2$	Laminar flow	Mandeville et al. (1999)
21	$\beta = 1.6$ taken 2 in the model	Vascular compliance parameter	Huppert et al. (2007)
21	$V_{v,0} = 0.0237$	Initial venous volume fraction	Buxton et al. (1998)
21	$F_{in,0} = 0.0217\ s^{-1}$	Initial flow in	Buxton et al. (1998)
23	$O_{2a} = 8.34$ mM	Total arterial oxygen concentration	Vafaee and Gjedde (2000)
24b	$M = 0.25$	*M*-value	Pasley et al. (2007)
24b	$\beta' = 1.5$	Imaging parameter	Davis et al. (1998)

This voltage change is then used to obtain the voltage-dependent Na^+ and Ca^{2+} channel activations. The Na^+ influx $[\nu_{Na^+}(t)]$ as a function of voltage and time is obtained by the Hodgkin–Huxley equations (Hodgkin and Huxley, 1952). The current calculated using Hodgkin–Huxley equations is then converted from μA/cm^2 to mmol/L s considering a 5-μm radii spherical cell.

Calcium influx in the neuron is mediated through *N*-methyl-D-aspartate receptor (NMDAR) channels that are voltage dependent (Shouval et al., 2002). This influx, the rate of Ca^{2+} concentration change in the neuron $(\nu_{Ca^{2+},n})$, is given as a product of the fraction of NMDARs that move from the closed to open state after each presynaptic action potential, the peak NMDA receptor conductance and the membrane potential (please see Shouval et al., 2002 for a detailed description of the equations and parameters).

The rate of intracellular sodium concentration change $[\nu_{Na^+}(t)]$, is used as an input to the metabolic rate equations described in Section 'Results'. The rate of intracellular calcium concentration change $(\nu_{Ca^{2+},n})$, is used in the production of NO as described below.

A BRIEF DESCRIPTION OF AUBERT AND COSTALAT'S MODEL OF STIMULUS INDUCED CHANGES IN OXYGEN CONSUMPTION

The portion of Aubert and Costalat's model (Aubert and Costalat, 2002) that we utilize here couples ionic current (Na ion flux) to brain energy metabolism (glycolysis, mitochondrial respiration and the phosphocreatine buffer). An increase in intracellular Na^+ activates the Na^+–K^+ pump and consumes more ATP. To compensate for the ATP decrease, the cell produces ATP through glycolysis, mitochondrial respiration and the phosphocreatine buffer. The following equation from the work of Aubert et al., (2007), which is based on the respiratory chain equation from Holzhütter et al. (1985), is used to describe the $CMRO_2$ (or ν_{mito}) in the model. The description and values of the parameters V, nop, Km_{ADP}, kr, phi, phi_0, H, H_m and nr can be found in Aubert et al. (2007).

$$CMRO_2 = V\left(\frac{ADP^{nop}}{ADP^{nop} + Km_{ADP}}\right)\left(\frac{kr}{1+phi}\right)\left(\frac{O_{2n}}{O_{2n} + qr.phi}\right), \quad (3a)$$

$$phi = phi_0\left(\frac{NAD}{NADH}\right)^{0.5}, \quad (3b)$$

$$phi_0 = pr\left(\frac{H}{H_m}\right)^{nr/2}, \quad (3c)$$

This oxygen consumption modulates the oxygen concentration in the tissue, altering the concentration gradient with respect to the blood vessel (Eq. 28 of Aubert and Costalat, 2002), thus changing the rate of oxygen extraction from the vessel (Eq. 43 of Aubert and Costalat, 2002).

CO_2 KINETICS

The carbon dioxide concentration in the neuron increases with mitochondrial respiration and decreases with CO_2 diffusion from the neuron to the precapillary arterioles via the concentration gradient,

$$\frac{dCO_{2n}}{dt} = n_{Aero}\nu_{mito} - \frac{V_{cap}}{V_n}\nu_{CO_{2nc}}. \quad (4)$$

The mitochondrial respiration rate (ν_{mito}) is given by Eq. 23 from Aubert et al. (2007). According to the brain tissue compartmentalization assumption of Aubert and Costalat (2002), V_{cap} and V_n are the volume fractions of the precapillary arterioles and neurons in the brain respectively, and n_{Aero} is the stoichiometric constant. The rate of CO_2 diffusion from the neuron to the precapillary arterioles ($\nu_{CO_{2nc}}$) is given by:

$$\nu_{CO_{2nc}} = D_{new,CO_2}\frac{1}{V_{cap}}\left(CO_{2n} - CO_{2c}\right), \quad (5a)$$

$$D_{new,CO_2} = \frac{D_{CO_2}}{d_{eff}^2}, \quad (5b)$$

where D_{new,CO_2} is the effective diffusion rate depending on the CO_2 diffusion coefficient (D_{CO_2}) and effective distance that CO_2 diffuses (d_{eff}). CO_{2n} is the concentration of CO_2 in the neuron and CO_{2c} is the concentration of CO_2 in the precapillary arterioles.

This CO_2 diffusion increases CO_2 concentration in the precapillary arterioles that is cleared by the in-flowing blood from the artery,

$$\frac{dCO_{2c}}{dt} = \nu_{CO_{2nc}} - \nu_{CO_{2ca}}. \quad (6)$$

The rate of change of CO_2 in the precapillary arterioles due to the flowing blood is given by:

$$\nu_{CO_{2ca}} = 2F_{in}\frac{1}{V_{cap}}\left(CO_{2c} - CO_{2a}\right), \quad (7)$$

where CO_{2a} is the concentration of CO_2 in the upstream artery.

CA^{2+} AND NO KINETICS

Calcium concentration in the neuron varies with the difference between calcium influx into the cell and the calcium decay,

$$\frac{dCa_n^{2+}}{dt} = \nu_{Ca^{2+}} - \nu_{Ca^{2+}\,decay}. \quad (8)$$

Calcium influx ($\nu_{Ca^{2+}}$) is described in Section 'Materials and Methods'. The calcium decay rate ($\nu_{Ca^{2+}\,decay}$) is given by Majewska (Majewska et al., 2000),

$$\nu_{Ca^{2+}\,decay} = \frac{1}{\tau_{Ca^{2+}}}Ca_n^{2+}, \quad (9)$$

where Ca_n^{2+} is the calcium concentration in the neuron and $\tau_{Ca^{2+}}$ is the decay time constant.

NO concentration in the neuron is determined by the rate of NO production ($\nu_{NO,n}$), the diffusion of NO from the neuron to smooth muscle ($\nu_{NO,sm}$), and the decay of NO in the neuron ($\nu_{NO\,decay,n}$):

$$\frac{dNO_n}{dt} = +\nu_{NO,n} - \nu_{NO,sm} - \nu_{NO\,decay,n}. \quad (10)$$

NO production is related to neuronal calcium concentration by Takahashi and Mendelsohn (2003), assuming that the maximum neuronal NO release is obtained during the maximal activation of nitric oxide synthase (Luiking and Deutz, 2003),

$$\nu_{NO,n} = 0.0053\left(Ca_n^{2+}\right)^{0.4066}. \quad (11)$$

The NO produced in the neuron then diffuses to the smooth muscle cells around arterioles:

$$\nu_{NO,sm} = D_{new,NO}\left(NO_n - NO_{sm}\right), \quad (12a)$$

$$D_{new,NO} = \frac{D_{NO}}{d_{eff}^2}, \quad (12b)$$

where $D_{new,NO}$ is the effective diffusion rate depending on the NO diffusion coefficient (D_{NO}) and the effective distance over which NO diffuses (d_{eff}). Some of the produced NO, on the other hand, is consumed by other reactions within the cell with a time constant (τ_{NO}) (Vaughn et al., 1998),

$$\nu_{NO\,decay,n} = \left(\frac{1}{\tau_{NO}}\right) NO_n. \tag{13}$$

NO concentration in smooth muscle is determined by the NO diffusion from the neuron ($\nu_{NO,sm}$) and the NO decay within the smooth muscle ($\nu_{NO\,decay,sm}$).

$$\frac{dNO_{sm}}{dt} = +\nu_{NO,sm} - \nu_{NO\,decay,sm}. \tag{14}$$

The NO decay in smooth muscle is given by Vaughn et al. (1998) as:

$$\nu_{NO\,decay,sm} = \left(\frac{1}{\tau_{NO}}\right) NO_{sm}. \tag{15}$$

where NO_{sm} is the NO concentration in smooth muscle.

Using the results of a mathematical model of the nitric oxide/cGMP pathway in the vascular smooth muscle cell (Yang et al., 2005), NO inhibition of calcium in smooth muscle is obtained via a fit:

$$Ca^{2+}_{sm} = -1785\,\text{nM}\ln\left(NO_{sm}\right) + 8630\,\text{nM}. \tag{16}$$

MODULATION OF VASCULAR TONE

We relate the arteriolar diameter to the pCO_2 in the precapillary arterioles using the information in Wang et al. (1992). Poiseuille's law states that the flow of blood through a vessel is proportional to the fourth power of the vessel diameter. Using the $PaCO_2$ versus CBF graph in Wang et al.'s work, we recalculated the $PaCO_2$ versus diameter graph with the assumption that 40 mmHg corresponds to the normal CO_2 levels in the vessel. We then fit a curve to this new graph and the curve fit formula is given in Eq. 17a where d_{CO_2} represents the fractional change in diameter. It well matches with former work of Muizelaar et al. where they find a relationship directly between $PaCO_2$ and diameter (Muizelaar et al., 1988).

$$d_{CO_2} = 6\times10^{-5}\,\text{mmHg}^{-2}\,P_{CO_2}{}^2 + 0.0027\,\text{mmHg}^{-1}\,P_{CO_2} - 0.2, \tag{17a}$$

$$P_{CO_2} = \frac{CO_{2c}}{\alpha_{CO_2}}. \tag{17b}$$

We have related CO_2 concentration to CO_2 partial pressure (P_{CO_2}) using the carbon dioxide solubility coefficient (α_{CO_2}) Baseline CO_2 pressure in the vessel is assumed to be 40 mmHg (Lumb, 2003).

The fractional diameter change of the arteriole related to NO production is obtained in terms of the smooth muscle calcium concentration (Ca_{sm}) using the data in Schuster et al.'s work (Schuster et al., 2001; Figure 4A). We selectively picked the diameter and calcium values at various time instances in the above mentioned work. We then converted this data into percentage change of diameter and calcium by normalizing it with the maximum fluorescence intensity. Then a new graph of diameter versus Ca was obtained to which a curve was fit to obtain Eq. 18a.

$$d_{NO} = \frac{631000}{460600 + \exp\left(12\left\|Ca^{2+}_{sm}\right\|\right)} \tag{18a}$$

$$\left\|Ca^{2+}_{sm}\right\| = \frac{Ca^{2+}_{sm}}{Ca^{2+}_{sm,max}} \tag{18b}$$

where the value of $Ca^{2+}{}_{sm,max}$ is given in **Table 2**.

The vascular radii (in units of meters) is then calculated by simple addition of the CO_2 effect (Eq. 17a) and the NO effect (Eq. 18a),

$$R = 5\times10^{-6}\,\text{m}\left(1 + d_{NO} + d_{CO_2}\right) \tag{19}$$

MODEL OUTPUTS: FLOW, VENOUS VOLUME, DEOXY-HEAMOGLOBIN CONCENTRATION AND BOLD SIGNAL

In the model, a hypothetical brain volume is formed to include a neuron, pre-capillary arteriole and venous compartments that are forming a unit voxel. Assuming the total BOLD signal being a volume-weighted sum of the signals coming from individual voxels (Buxton et al., 1998) and using Davis' equation (Davis et al., 1998) which links normalized $CMRO_2$ and CBF changes to the BOLD signal change, we can then calculate the percent change in BOLD signal within a voxel due to neuronal activation. Hence, the CBF, CBV and BOLD are calculated as follows:

The flow (F_{in}) in the precapillary arteriole is calculated using the Poiseuille equation with the parameters: radii (R), pressure difference across the two ends of the precapillary arteriole (ΔP), viscosity of the blood (μ) and the length of the vessel (L). We have normalized this flow with arteriole volume in order to have dimensions consistent with Aubert's model (Aubert and Costalat's, 2002).

$$F_{in} = \frac{\pi R^4 \Delta P}{8\mu L V_{arteriole}}, \tag{20a}$$

$$V_{arteriole} = \pi R^2 L. \tag{20b}$$

The output flow from the venous compartment is obtained from the following equation (Mandeville et al., 1999; Boas et al., 2003):

$$F_{out} = \frac{V_v^{\alpha+\beta}}{V_{v,0}^{\alpha+\beta}} F_{in,0}. \tag{21}$$

In Eq. 21 we assume laminar flow ($\alpha = 2$), and constant β represents diminished volume reserve at elevated pressures. We are using $\beta = 2$ as representative of the range of $1 \le \beta \le 3$ from the literature (Mandeville et al., 1999; Huppert et al., 2007).

The following equation (Buxton et al., 1998) is used for venous volume calculations,

$$\frac{dV_v}{dt} = F_{in} - F_{out}, \tag{22}$$

where F_{in} and F_{out} are calculated using Eqs. 20a and 21.

The deoxy-Heamoglobin (dHb) concentration and the BOLD signal are calculated by Buxton et al. (1998), Davis et al. (1998), respectively:

$$\frac{d\mathrm{dHb}}{dt} = 2F_{\mathrm{in}}\left(\mathrm{O}_{2a} - \mathrm{O}_{2c}\right) - F_{\mathrm{out}}\frac{\mathrm{dHb}}{V_{\mathrm{v}}} \tag{23}$$

$$\mathrm{BOLD} = \frac{\Delta S}{S_0} \tag{24a}$$

$$\frac{\Delta S}{S_0} = M\left[1 - \left(\frac{\mathrm{CMRO}_2}{\mathrm{CMRO}_{2,0}}\right)^{\beta'}\left(\frac{\mathrm{CBF}}{\mathrm{CBF}_0}\right)^{\alpha-\beta'}\right] \tag{24b}$$

with the parameters O_{2a}, M and β' given in **Table 2**. O_{2c} is the pre-capillary arteriole oxygen concentration.

SOLVING THE ORDINARY DIFFERENTIAL EQUATIONS

The model is comprised of 20 variables. Volumes, areas and CBF values are all expressed per unit tissue volume. In order to solve the ordinary differential equations, we have used the ode23s tool of MATLAB7.5 for stiff equations. Besides the equations given in sections above, the first 13 equations in **Table 1** in Aubert's model (Aubert and Costalat, 2002) are used in this model with the corresponding parameters within the same work.

ASSUMPTIONS

We set CBF dependent solely on radii changes with the assumption that the local CBF changes in precapillary arterioles are dependent more on diameter changes of the vessels than the pressure difference between the two ends of them, which may not be the case during systemic changes (heart rate, stroke volume etc.) activated during brain function.

We have also assumed that the NO and CO_2 effect on blood flow are independent of each other. Although previous research on rats suggest that inhibition of nitric oxide synthase reduces the CBF response to hypercapnia (Wang et al., 1995), more recent research on humans found no significant change in CBF response to hypercapnia under NOS inhibitors (White et al., 1998). We base our model on this more recent finding.

The fourth assumption to be mentioned here is that the energy consumption during brain activation is solely due to the Na^+–K^+ pump. Actually when the Na^+–K^+-ATPase is blocked in the whole brain, the energy usage drops dramatically (Riera et al., 2008), a fact which makes this assumption acceptable.

We modeled the action of NO and Ca on pre-capillary arterioles since they have smooth muscle cells which dilate actively by using NO and Ca signaling pathways.

We have also assumed that Ca entry into channels is solely through NMDA channels. Our assumption is based on the studies which show that calcium elevation due to synaptic activity is almost totally blocked in the presence of NMDA channel blocker AP5 (Müller and Connor, 1991; Alford et al., 1993; Malinow et al., 1994).

RESULTS

We plot Ca^{2+} and Na^+ dynamics in the neuron as a response to a stimulus lasting 20 and 100 s (**Figure 2**). A sample part from the stimulus in **Figure 2A**, shows the change in membrane voltage, i.e. action potentials, during the stimuli.

To explore the relative roles of the vasoactive agents NO and CO_2 in the stimulus evoked change in CBF, in **Figure 3** we plot the relative change in CBF (rCBF) for a short (20 s) and long (100 s) duration stimulus considering modulation of the vascular tone by NO only, CO_2 only, and both NO and CO_2.

The largest change in CBF is observed with NO only, while CO_2 alone is producing only a small increase in CBF. When both NO and CO_2 effects on vascular tone are considered, the CBF response is reduced relative to NO alone. We observe a flow overshoot during the first 10 s of the stimulus, a significant post-stimulus undershoot for the short stimulus, and a slow post-stimulus recovery for the long-stimulus. These results reveal that the vessels may dilate or constrict depending on the balance of CO_2 production by the mitochondria and washout by the flowing blood.

In **Figure 4** we plot the evoked changes in the BOLD signal corresponding to the differing flow responses from NO only, CO_2 only, and both NO and CO_2 modification of vascular tone. Inhibiting the effect of NO significantly reduces the flow response (see **Figure 3**) leading to a negative BOLD response as the reduced flow response does not oversupply the increased demand for oxygen. Considering the effects of both NO and CO_2 compared with NO alone attenuates the peak BOLD response during the stimulus and modifies the post-stimulus BOLD undershoot, increasing the undershoot for a short stimulus and diminishing its duration for long stimulus. This modification of the post-stimulus BOLD undershoot is due to a slow $CMRO_2$ recovery and the post-stimulus flow undershoot.

The precapillary arteriole pCO_2 pressure corresponding to the three different vasoactive effects is plotted in **Figure 5**. It is evident that the large flow response produced by NO is washing out more CO_2 than is being produced by the increased oxygen consumption, causing a reduction in the pCO_2 akin to the washout of deoxygenated hemoglobin during a stimulus. When the effect of NO on vascular tone is neglected, we observe that the pCO_2 increases because the flow response is too small to wash out the extra CO_2 produced by the increased oxygen consumption, consistent with the negative BOLD signal in **Figure 4**. We also observe a post-stimulus overshoot in the pCO_2 arising from the slow recovery of oxygen consumption.

To provide support for the magnitude of the CO_2 effect in varying vascular tone in our model, we simulated the change in flow and BOLD as the systemic pCO_2 was increased, and compared our simulation results with experimental results. The simulated results are shown in **Figure 6** compared with experimental data from Kety and Schmidt (1948), Grubb et al. (1974) and Hoge et al. (1999b). Our model results well match with the experimentally observed flow changes and the BOLD changes.

In **Figure 7A**, we plot the peak value of the post-stimulus CBF undershoot versus stimulus duration as predicted by our model compared with a survey of experimental data from the literature (Hoge et al., 1999b; Kim et al., 1999; Krüger et al., 1999; Rosengarten et al., 2001; Lu et al., 2004; Uludağ et al., 2004). We considered only human visual stimulation experiments for this comparison. The

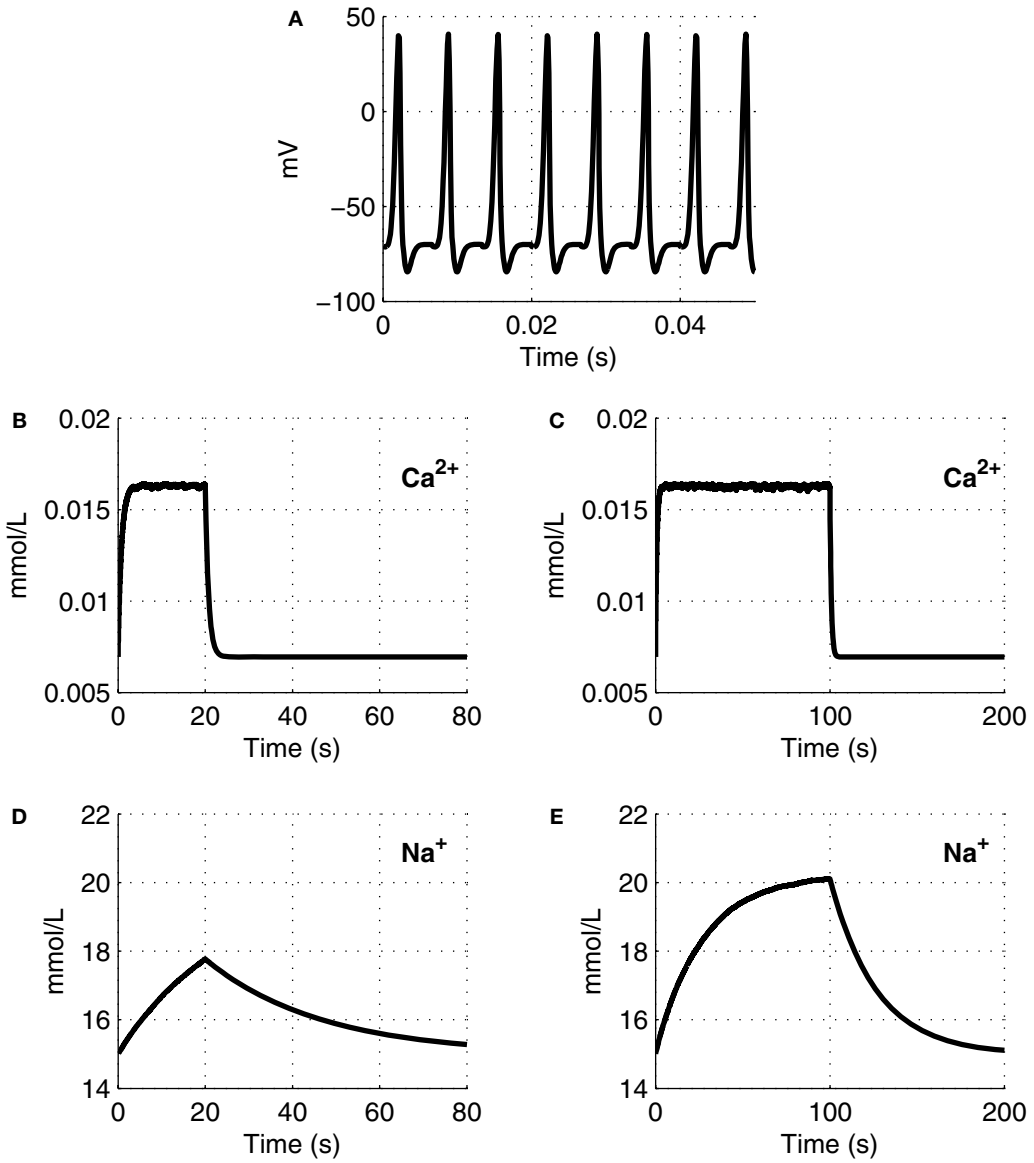

FIGURE 2 |The input function of the model: a series of action potentials at 150 Hz (A), only a portion is shown as an example. The Ca^{2+} and Na^{+} concentration as a response to the stimulus. Results are given **(B)** and **(D)** for a 20-s stimulus and **(C)** and **(E)** for a 100-s stimulus.

specific studies and their associated data points are provided in **Table 3**. For both experimental studies and our model, the CBF undershoot reaches a maximum for a stimulus duration of ~20 s, and slowly diminishes for longer duration stimuli.

Finally, we plot our model prediction of the post-stimulus BOLD undershoot versus stimulus duration in **Figure 7B** compared with a survey of experimental data from the literature in **Table 4** (Hoge et al., 1999a; Krüger et al., 1999; Royl et al., 2001). Our results show that BOLD undershoot increases during the first 50 s of stimulus duration and then reaches a plateau around 100 s, while the literature suggests that the plateau is reached around 30 s and at a much smaller amplitude. We note that we obtain better agreement between the model and experimental data if we force the model to have a faster $CMRO_2$ increase following stimulus onset and recovery post-stimulus.

We have performed a sensitivity analysis to verify the robustness of the CBF post-stimulus behavior shown in **Figure 3**. The decay constants for Ca and NO were varied over their physiological range ($\tau_{Ca^{2+}}$: 0.5–1 s, Göbel and Helmchen, 2007, τ_{NO}: 0.5–5 s, Vaughn et al., 1998). While there was a dramatic decrease in the CBF undershoot as we increased $\tau_{Ca^{2+}}$, we none-the-less still observe an undershoot at $\tau_{Ca^{2+}} = 1$ s. We observed that τ_{NO} had no significant effect on the CBF undershoot. In addition, the diffusion constants for NO (3.3×10^{-5} to 4.8×10^{-5} cm^2/s; Seraya and Nartsissov, 2002; Kavdia and Popel, 2004) and CO_2 (1.14×10^{-5} to 2.5×10^{-5}; Geers and Gros, 2000) have a negligible effect on the undershoot results. Increasing the maximum Na conductance (g_{Na}) decreases the undershoot, completely abolishing it when $g_{Na} > 15$ mS/cm^2 (we used 4.4 mS/cm^2 in **Figure 7**; Meyer et al.,

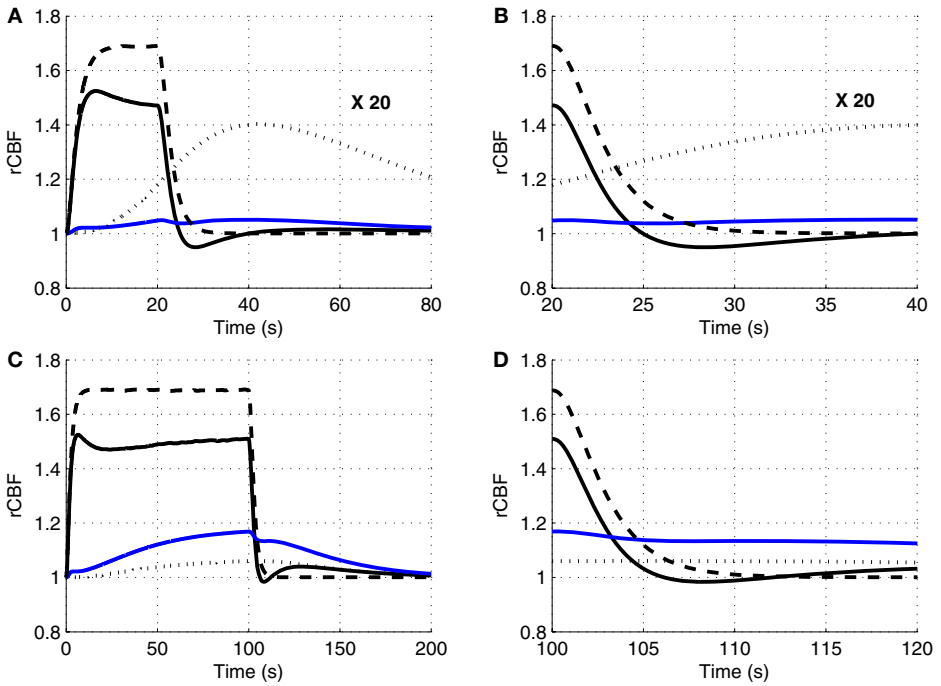

FIGURE 3 | Our model results for an evoked change in CBF considering the vasoactive role of only NO (dashed line), only CO_2 (dotted line), both NO and CO_2 (solid line). The relative change in $CMRO_2$ is indicated by the blue line. Results are given **(A)** and **(B)** for a 20-s stimulus and **(C)** and **(D)** for a 100-s stimulus. In each case we considered the stimulus as a train of action potentials at a repetition frequency of 150 Hz as input to our model. Note that in **(A)** we increased the scale of the only CO_2 effect (dotted line) by ×20. CBF, cerebral blood flow; $CMRO_2$, cerebral metabolic rate of oxygen.

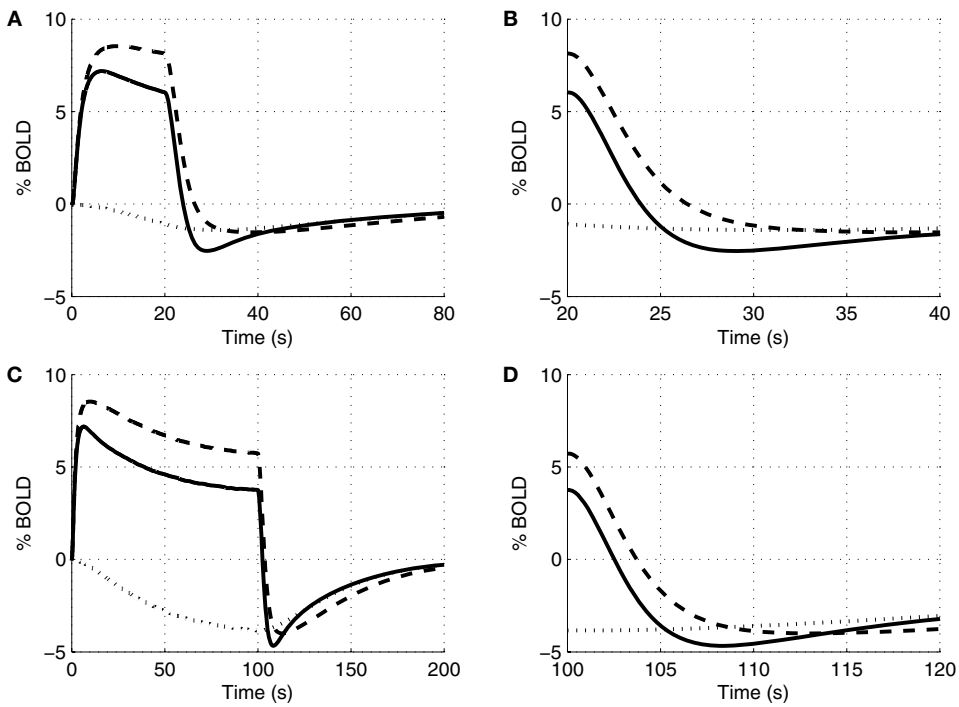

FIGURE 4 | Our model results for an evoked change in BOLD considering the vasoactive role of only NO (dashed line), only CO_2 (dotted line), and both NO and CO_2 (solid line). Results are given **(A)** and **(B)** for a 20-s stimulus and **(C)** and **(D)** for a 100-s stimulus. In each case we considered the stimulus as a train of action potentials at a repetition frequency of 150 Hz as input to our model. BOLD, blood oxygenation level-dependent.

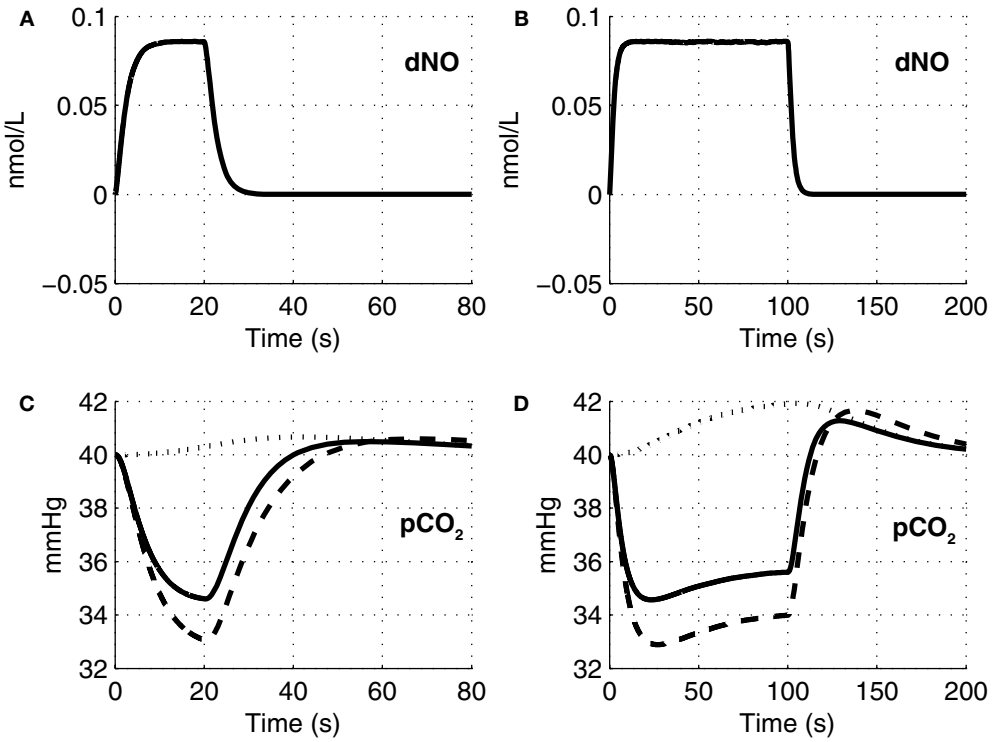

FIGURE 5 | Change in NO levels in smooth muscle (A,B) and the partial pressure of CO_2 in the precapillary arteriole (C,D) are plotted considering the flow response from NO alone (dashed line), CO_2 alone (dotted line), and both NO and CO_2 (solid line) for the 20-s stimulus (A,C) and the 100-s stimulus (B,D). pCO_2, partial pressure of CO_2.

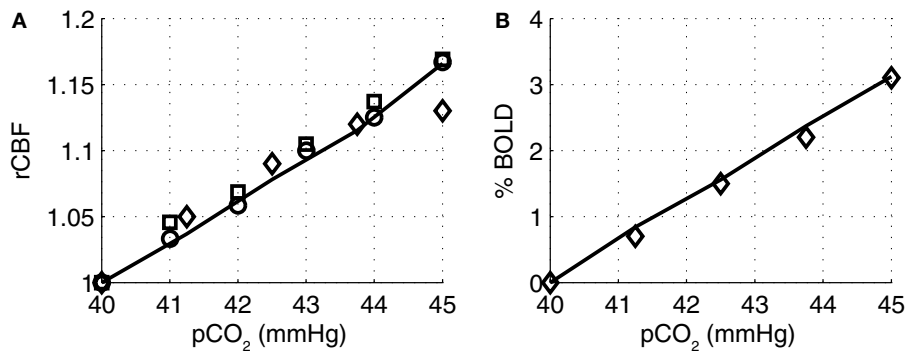

FIGURE 6 | Modeled (A) CBF and (B) BOLD versus the partial pressure of CO_2 compared with experimental data from (Kety and Schmidt, 1948) circles, (Grubb et al., 1974) squares, and (Hoge et al., 1999b) diamonds. Our model results are indicated by the solid line. CBF, cerebral blood flow; BOLD, blood oxygenation level-dependent.

1997). Varying NMDA conductance (g_{NMDA}) had no effect on the undershoot over the range of 500–1350 μM/(ms mV) (Shouval et al., 2002).

DISCUSSION

The results of our model confirm the expected dominant vasodilatory role of NO, however CO_2 is also important in modulating the shape of the response, in particular the initial overshoot and post-stimulus undershoot. Our results indicate that a washout of CO_2 has a vasoconstrictive effect throughout the stimulus because NO dominates the blood flow response. While the vasoactive role of NO in producing a blood flow response is known experimentally (Morikawa et al., 1992; Iadecola et al., 1993; Akgören et al., 1994), there is no experimental support for the possible blood flow effects of locally-produced-CO_2.

The transient increase in nitric oxide, as reported in the literature, varies widely. While there are some studies showing the change to be as low as 2.2 nM in rats after parallel fiber stimulation

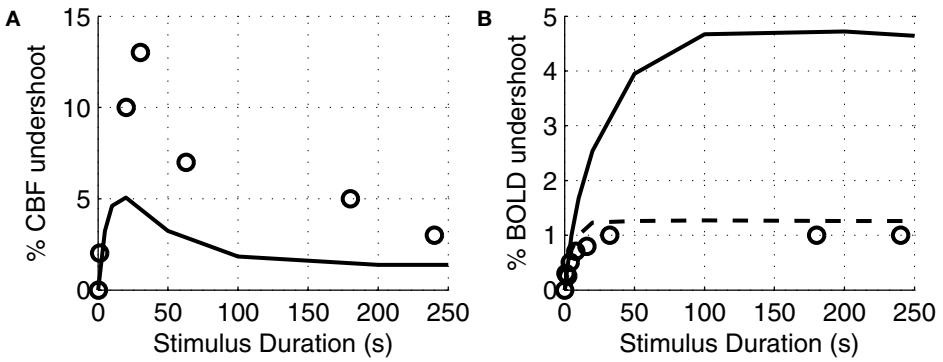

FIGURE 7 | Peak CBF undershoot versus stimulus duration (A). BOLD undershoot versus stimulus duration **(B)**. Experimental data (circles), model results (solid line), model results when the model is forced to have a faster $CMRO_2$ increase following stimulus onset and recovery post-stimulus (dotted-line). CBF, cerebral blood flow.

Table 3 | Peak percentage CBF undershoot at various stimulus durations in literature.

Stimulus duration (s)	% CBF undershoot	Reference
1	2	(10 Hz) Rosengarten et al. (2001)
20	10	(8 Hz) Uludağ et al. (2004)
30	13	(8 Hz) Lu et al. (2004)
63	7	(8 hz) Kim et al. (1999)
180	5	(4 Hz) Hoge et al. (1999a)
240	3	(5 Hz) Krüger et al. (1999)

Table 4 | Peak percentage BOLD undershoot at various stimulus durations in literature.

Stimulus duration (s)	% BOLD undershoot	Reference
1	0.3	Royl et al. (2001)
2	0.25	Royl et al. (2001)
4	0.5	Royl et al. (2001)
8	0.7	Royl et al. (2001)
16	0.8	Royl et al. (2001)
32	1	Royl et al. (2001)
180	1	Hoge et al. (1999a)
240	1	Krüger et al. (1999)

(Kimura et al., 1998) and 0.3 nM in cat nucleus tractus solitarius after arginine application (Wu et al., 2002), some values are as high as 80 nM in cat after visual stimulus (Buerk et al., 1996) and 200 nM in rats after forepaw stimulus (Buerk et al., 2003). We also varied the decay constants for NO over their physiological range τ_{NO}: 0.5–5 s (Vaughn et al., 1998). Our sensitivity analysis showed that τ_{NO} had no significant effect on the CBF undershoot. The shape of the reported NO responses also varies as stimulus type changes. The shape of the NO change in our model is more similar to the experimentally measured response for a visual stimulus (Buerk et al., 1996), than for a forepaw stimulus (Buerk et al., 2003).

A post-stimulus CBF undershoot has been observed by numerous groups. Specifically, the CBF undershoot has been observed in rat somatosensory cortex (Lindauer et al., 1993; Kida et al., 2007), cat visual cortex (Jin and Kim, 2008), and human visual cortex (Hoge et al., 1999a; Kim et al., 1999; Lu et al., 2004; Uludağ et al., 2004; Chen and Pike, 2009). Our simulations also result in a post-stimulus CBF undershoot. Our results show that the interplay between NO and CO_2 is a possible explanation for this undershoot, without ruling out the effect of other possible confounding mechanisms such as neuronal inhibition.

Although there is no direct evidence for a hypocapnic vasoconstrictive effect of CO_2 washout during brain activation in the literature, our model provides a novel explanation for features of the CBF response observed in the literature. Inspecting the components of the CBF response for short and long stimuli, we observe a post-stimulus undershoot for short stimulus while we see only a very brief and small undershoot for the long duration stimulus which is subsequently followed by a slow positive CBF recovery. For short stimuli, the increase in CBF during the stimulus has washed-out more CO_2 than is being produced by the increased oxygen consumption. This reduces tissue pCO_2 such that when the NO vasodilation returns to baseline post-stimulus, the reduced pCO_2 results in vasoconstriction and an undershoot in CBF (see **Figure 5C**). For longer stimuli, the oxygen consumption increase is greater and takes a long time to recover post-stimulus. Thus more CO_2 is produced than is being washed away, allowing pCO_2 to increase relative to baseline and return slowly to baseline as oxygen consumption returns to baseline (see **Figure 5D**). This results in dilated vessels and a slowly recovering positive increase in CBF. These model results are consistent with a CBF undershoot observed experimentally following a 20 s stimulation of the occipital cortex by a flickering radial checkerboard (Uludağ et al., 2004). Kim et al. found a modest undershoot in the primary visual cortex under 63 s of red/black reversing circular checkerboard stimulus (Kim et al., 1999). In a similar experiment with a longer stimulus duration (3 min), a mild CBF undershoot is observed in primary visual cortex under low-contrast radial checkerboard (Hoge et al., 1999a), which are all consistent with the results of the model (see **Figure 7A**). The model underestimates the experimental data which may be due to other possible mechanisms leading to CBF undershoot which are not considered in the model such as neuronal inhibition.

Our model also provides a novel explanation for an initial CBF overshoot during the first 10 s of a stimulus (see **Figure 3**) as observed by Krüger et al. (1999) arising from CO_2 dynamics

rather than neuronal habituation. During the initial few seconds of the stimulus, the CBF response is dominated by the NO effect. This increase in CBF, washes out CO_2, the vessels constrict slightly because of the reduced pCO_2, and thus CBF reduces slightly from the increased vascular resistance. Interestingly, closer inspection of our results for the longer duration stimulus (**Figure 3C**) shows a subsequent increase in CBF after reaching a minimum at 20 s, consistent with Hoge et al. (1999a), Krüger et al. (1999). This secondary increase in CBF arises from oxygen consumption continuing to increase during the stimulus, producing more CO_2 (see **Figure 5D**), dilating the vessels, and increasing CBF.

The positive BOLD response is determined by the relative contributions of CBV, CBF and $CMRO_2$. When the effect of only NO and both NO and CO_2 are considered, a positive BOLD response is obtained during the stimulus. Inhibiting the effect of NO diminishes the CBF increase significantly and so results in a negative BOLD response due to the insufficient oxygen supply to the activation area. This result is supported by various experimental efforts to determine the effect of NO in neurovascular coupling. Stevanovic et al. showed that inhibiting nitric oxide synthase significantly attenuates the CBV, CBF and BOLD responses (Stefanovic et al., 2007). Since this inhibition of nitric oxide is not 100%, and it also diminishes the neural activation though less strongly, they still obtained a very low but still positive BOLD response. Findings from other works also suggest that the positive BOLD response is abolished by the inhibition of nitric oxide (Burke and Bührle, 2006).

For the post-stimulus BOLD undershoot, three mechanisms have been suggested:

(1) sustained oxygen consumption after CBF has returned to baseline (Frahm et al., 1996; Schroeter et al., 2006),
(2) a slow recovery of CBV to baseline compared to CBF (Mandeville et al., 1999), and
(3) a post-stimulus CBF undershoot (Hoge et al., 1999a).

Our model results suggest that the BOLD undershoot for short stimuli is mostly due to a CBF undershoot that arises from a reduced pCO_2. Experimental data supporting the BOLD undershoot due to a CBF undershoot resulting from reduced pCO_2 levels can be found in a recent work by Wise et al. (2007). In their work, the end-tital CO_2 undershoot, after a fixed-inspired hypercapnic challenge, precedes the BOLD undershoot. Although they do not show the CBF transients, a possible explanation for this is that, the CBF, before returning to baseline, washed-out the pCO_2 below the baseline levels, and this, in response, caused an undershoot in CBF. For long stimuli, on the other hand, the post-stimulus BOLD undershoot in our model arises from a sustained oxygen consumption slowly recovering to baseline. Although this sustained oxygen consumption raises pCO_2 above baseline, resulting in an increase in CBV, this does not enhance the post-stimulus BOLD undershoot because the elevated pCO_2 also increases CBF washing out more CO_2 and deoxygenated hemoglobin. Our model results support the combined roles of a flow undershoot and a sustained post-stimulus increase in $CMRO_2$ in producing a BOLD undershoot, with the former dominating for short-stimuli and the latter for longer duration stimuli. We also want to point out that we have assumed a flow-volume relationship, which discarded any possible BOLD undershoot that could be produced by a slow volume recovery. The BOLD undershoot in our model would be enhanced by a slow volume recovery. We also note that our model does not comment on the possible role of active vasoconstriction related to inhibitory signals as recently suggested in Devor et al. (2007). Finally, the relative contributions of these different mechanisms of vasoregulation will likely be altered in cerebrovascular disease.

In addition, the model's slow $CMRO_2$ onset and recovery dynamics require further support. We used in the model the $CMRO_2$ kinetics given in Aubert et al., (2007), which is based on the respiratory chain equation from the work of Holzhütter et al. (1985). The slow onset kinetics in $CMRO_2$ used in this model is controversial and should be discussed. For example, a PET study from Mintun et al showed a 4.7% increase in $CMRO_2$ 60 s after the stimulus onset, while this value reaches 15% after 25 min of stimulation (Mintun et al., 2002). A recent work from Lin et al. also obtained slow $CMRO_2$ onset kinetics using fMRI (Lin et al., 2009). The work of Prichard et al. confirms this slow increase in $CMRO_2$, showing a slow lactate decay after the onset of photic stimulation (Prichard et al., 1991). In contrary, other recent works show a much faster increase in $CMRO_2$ (Davis et al., 1998; Maciejewski et al., 2004; Shen et al., 2008; Wu et al., 2009). For example; Wu et al. calculated the $CMRO_2$ from CBF and BOLD signals using a biophysical model. They obtained a $CMRO_2$ increase, reaching a steady state within a few seconds as a response to visual stimulation. We tried different $CMRO_2$ onset kinetics in our model to see the possible changes in our results (data not shown). The BOLD percentage increase was lower for the fast kinetics than for the slow kinetics, and in better agreement with literature. The $CMRO_2$ onset kinetics also has an effect on tissue pO_2. With a slow onset we do not observe any transient decrease in tissue pO_2 (data not shown), as opposed to the existing literature on the topic (Ances et al., 2001; Offenhauser et al., 2005). This is also supported by two recent studies, which use pharmacological agents to eliminate the blood flow response, and measure the BOLD signal in response to stimulation as an indicative of $CMRO_2$. Time to peak values obtained by these studies are around 10 s, supporting a faster $CMRO_2$ onset kinetics (Nagaoka et al., 2006; Zappe et al., 2008). However, the increasing kinetics for $CMRO_2$ did not have much of an effect on the CBF onset, and CBF and BOLD post-stimulus transients, the parameters altering the shaping of the hemodynamic response on which we have focused our discussion.

In summary, the increase in CBF during stimulation likely reduces local tissue pCO_2. This is another possible explanation for the post-stimulus CBF undershoot that has been described in the literature. It should also be added that the relative contributions of these different mechanisms of vasoregulation will likely be altered in cerebrovascular diseases.

ACKNOWLEDGMENTS

We would like to acknowledge Tamer Demiralp, Sava Sakadžić, Qianqian Fang, Uzay Emrah Emir and Rickson Coelho Mesquita for their helpful comments. This work is funded by TUBITAK-BAYG and NIH (R01NS-057476, P01NS-055104 and R01NS-051188).

REFERENCES

Akgören, N., Fabricius, M., and Lauritzen, M. (1994). Importance of nitric oxide for local increases of blood flow in rat cerebellar cortex during electrical stimulation. *Proc. Natl. Acad. Sci. U.S.A.* 91, 5903–5907.

Akın, A., Bilensoy, D., Emir, U. E., Gülsoy, M., Candansayar, S., and Bolay, H. (2006). Cerebrovascular dynamics in patients with migraine: near-infrared spectroscopy study. *Neurosci. Lett.* 400, 86–91.

Alford, S., Frenguelli, B. G., Schofield, J. G., and Collingridge, G. L. (1993). Characterization of Ca^{2+} signals induced in hippocampal CA1 neurones by the synaptic activation of NMDA receptors. *J. Physiol. (Lond.)* 469, 693–716.

Ances, B. M., Buerk, D. G., Greenberg, J. H., and Detre, J. A. (2001). Temporal dynamics of the partial pressure of brain tissue oxygen during functional forepaw stimulation in rats. *Neurosci. Lett.* 306, 106–110.

Aubert, A., and Costalat, R. (2002). A model of the coupling between brain electrical activity, metabolism, and hemodynamics: application to the interpretation of functional neuroimaging. *Neuroimage* 17, 1162–1181.

Aubert, A., and Costalat, R. (2005). Interaction between astrocytes and neurons studied using a mathematical model of compartmentalized energy metabolism. *J. Cereb. Blood Flow Metab.* 25, 1476–1490.

Aubert, A., Pellerin, L., Magistretti, P. J., and Costalat, R. (2007). A coherent neurobiological framework for functional neuroimaging provided by a model integrating compartmentalized energy metabolism. *Proc. Natl. Acad. Sci. U.S.A.* 104, 4188–4193.

Banaji, M., Tachtsidis, I., Delpy, D., and Baigent, S. (2005). A physiological model of cerebral blood flow control. *Math. Biosci.* 194, 125–173.

Bean, P. B. (2007). The action potential in mammalian central neurons. *Nat. Rev. Neurosci.* 8, 451–465.

Boas, D. A., Strangman, G., Culver, J. P., Hoge, R. D., Jasdzewski, G., Poldrack, R. A., Rosen, B. R., and Mandeville, J. B. (2003). Can the cerebral metabolic rate of oxygen be estimated with near-infrared spectroscopy? *Phys. Med. Biol.* 48, 2405–2418.

Buerk, D. G., Ances, B. M., Greenberg, J. H., and Detre, J. A. (2003). Temporal dynamics of brain tissue nitric oxide during functional forepaw stimulation in rats. *Neuroimage* 18, 1–9.

Buerk, D. G., Riva, C. E., and Cranstoun, S. D. (1996). Nitric oxide has a vasodilatory role in cat optic nerve head during flicker stimuli. *Microvasc. Res.* 52, 13–26.

Burke, M., and Bührle, Ch. (2006). BOLD response during uncoupling of neuronal activity and CBF. *Neuroimage* 32, 1–8.

Buxton, R. B., Wong, E. C., and Frank, L. R. (1998). Dynamics of blood flow and oxygenation changes during brain activation: the balloon model. *Magn. Reson. Med.* 39, 855–864.

Cabrales, P., Tsai, A. G., Winslow, R. M., and Intaglietta, M. (2005). Effects of extreme hemodilution with hemoglobin-based O2 carriers on microvascular pressure. *Am. J. Physiol. Heart Circ. Physiol.* 288, H2146–H2153.

Chen, J. J., and Pike, G. B. (2009). Origins of the BOLD post-stimulus undershoot. *Neuroimage* 46, 559–568.

Chen, Q., and Anderson, D. R. (1997). Effect of CO2 on intracellular pH and contraction of retinal capillary pericytes. *Invest. Ophthalmol. Vis. Sci.* 38, 643–651.

Clark, V. P., Lai, S., and Deckel, A. W. (2002). Altered functional MRI responses in Huntington's disease. *Neuroreport* 13, 703–706.

Davis, T. L., Kwong, K. K., Weisskoff, R. M., and Rosen, B. R. (1998). Calibrated functional MRI: mapping the dynamics of oxidative metabolism. *Proc. Natl. Acad. Sci. U.S.A.* 95, 1834–1839.

Devor, A., Tian, P., Nishimura, N., Teng, I. C., Hillman, E. M., Narayanan, S. N., Ulbert, I., Boas, D. A., Kleinfeld, D., and Dale, A. M. (2007). Suppressed neuronal activity and concurrent arteriolar vasoconstriction may explain negative blood oxygenation level-dependent signal. *J. Neurosci.* 27, 4452–4459.

Drake, C. T., and Iadecola, C. (2007). The role of neuronal signaling in controlling cerebral blood flow. *Brain Lang.* 102, 141–152.

Estrada, C., and DeFelipe, J. (1998). Nitric oxide-producing neurons in the neocortex: morphological and functional relationship with intraparenchymal microvasculature. *Cereb. Cortex* 8, 193–203.

Frahm, J., Krüger, G., Merboldt, K. D., and Kleinschmidt, A. (1996). Dynamic uncoupling and recoupling of perfusion and oxidative metabolism during focal brain activation in man. *Magn. Reson. Med.* 35, 143–148.

Freitas, R. A. Jr. (1999). Nanomedicine, Basic Capabilities. Georgetown, TX, Landes Bioscience.

Geers, C., and Gros, G. (2000). Carbon dioxide transport and carbonic anhydrase in blood and muscle. *Physiol. Rev.* 80, 2000.

Girouard, H., and Iadecola, C. (2006). Neurovascular coupling in the normal brain and in hypertension, stroke, and Alzheimer disease. *J. Appl. Physiol.* 100, 328–335.

Göbel, W., and Helmchen, F. (2007). In vivo calcium imaging of neural network function. *Physiology (Bethesda)* 22, 358–365.

Gros, G., and Moll, W. (1971). The diffusion of carbon dioxide in erythrocytes and hemoglobin solutions. *Pflugers Arch.* 324, 249–266.

Grubb, R. L., Raichle, M. E., Eichling, J. O., and Ter-Pogossian, M. M. (1974). The effects of changes in PaCO2 on cerebral blood volume, blood flow, and vascular mean transit time. *Stroke* 5, 630–639.

Hodgkin, A. L., and Huxley, A. F. (1952). A quantitative description of membrane current and its application to conduction and excitation in nerve. *J. Physiol. (Lond.)* 117, 500–544.

Hoge, R. D., Atkinson, J., Gill, B., Crelier, G. R., Marrett, S., and Pike, G. B. (1999a). Stimulus-dependent BOLD and perfusion dynamics in human V1. *Neuroimage* 9, 573–585.

Hoge, R. D., Atkinson, J., Gill, B., Crelier, G. R., Marrett, S., and Pike, G. B. (1999b). Linear coupling between cerebral blood flow and oxygen consumption in activated human cortex. *Proc. Natl. Acad. Sci. U.S.A.* 96, 9403–9408.

Holzhütter, H. G., Henke, W., Dubiel, W., and Gerber, G. (1985). A mathematical model to study short-term regulation of mitochondrial energy transduction. *Biochim. Biophys. Acta* 810, 252–268.

Huppert, T. J., Allen, M. S., Benav, H., Jones, P. B., and Boas, D. A. (2007). A multicompartment vascular model for inferring baseline and functional changes in cerebral oxygen metabolism and arterial dilation. *J. Cereb. Blood Flow Metab.* 27, 62–1279.

Iadecola, C., and Nedergaard, M. (2007). Glial regulation of the cerebral microvasculature. *Nat. Neurosci.* 10, 1369–1376.

Iadecola, C., Zhang, F., and Xu, X. (1993). Role of nitric oxide synthase-containing vascular nerves in cerebrovasodilation elicited from cerebellum. *Am. J. Physiol.* 264(Pt 2), R738–R746.

Irani, F., Platek, S. M., Bunce, S., Ruocco, A. C., and Chute, D. (2007). Functional near infrared spectroscopy (fNIRS): an emerging neuroimaging technology with important applications for the study of brain disorders. *Clin. Neuropsychol.* 21, 9–37.

Ito, H., Kanno, I., and Fukuda, H. (2005). Human cerebral circulation: positron emission tomography studies. *Ann. Nucl. Med.* 19, 65–74.

Jin, T., and Kim, S. G. (2008). Cortical layer-dependent dynamic blood oxygenation, cerebral blood flow and cerebral blood volume responses during visual stimulation. *Neuroimage* 43, 1–9.

Kavdia, M., and Popel, A. S. (2004). Contribution of nNOS- and eNOS-derived NO to microvascular smooth muscle NO exposure. *J. Appl. Physiol.* 97, 293–301.

Kety, S. S., and Schmidt, C. F. (1948). The effects of altered arterial tensions of carbon dioxide and oxygen on cerebral blood flow and cerebral oxygen consumption of normal young men. *J. Clin. Invest.* 27, 484–492.

Kida, I., Rothman, D. L., and Hyder, F. (2007). Dynamics of changes in blood flow, volume, and oxygenation: implications for dynamic functional magnetic resonance imaging calibration. *J. Cereb. Blood Flow Metab.* 27, 690–696.

Kim, S. G., Rostrup, E., Larsson, H. B., Ogawa, S., and Paulson, O. B. (1999). Determination of relative CMRO2 from CBF and BOLD changes: significant increase of oxygen consumption rate during visual stimulation. *Magn. Reson. Med.* 41, 1152–1161.

Kimura, S., Uchiyama, S., Takahashi, H. E., and Shibuki, K. (1998). cAMP-dependent long-term potentiation of nitric oxide release from cerebellar parallel fibers in rats. *J. Neurosci.* 18, 8551–8558.

Krüger, G., Kastrup, A., Takahashi, A., and Glover, G. H. (1999). Simultaneous monitoring of dynamic changes in cerebral blood flow and oxygenation during sustained activation of the human visual cortex. *Neuroreport* 10, 2939–2943.

Lin, A. L., Fox, P. T., Yang, Y., Lu, H., Tan, L. H., and Gao, J. H. (2009). Time-dependent correlation of cerebral blood flow with oxygen metabolism in activated human visual cortex as measured by fMRI. *Neuroimage* 44, 16–22.

Lindauer, U., Megow, D., Matsuda, H., and Dirnagl, U. (1999). Nitric oxide: a modulator, but not a mediator, of neurovascular coupling in rat somatosensory cortex. *Am. J. Physiol. Heart Circ. Physiol.* 277, H799–H811.

Lindauer, U., Villringer, A., and Dirnagl, U. (1993). Characterization of CBF response to somatosensory stimulation: model and influence of anesthetics. *Am. J. Physiol.* 264, H1223–H1228.

Lu, H., Golay, X., Pekar, J. J., and Zijl, P. J. M. (2004). Sustained poststimulus elevation in cerebral oxygen utilization after vascular recovery. *J. Cereb. Blood Flow Metab.* 24, 764–770.

Luiking, Y. C., and Deutz, N. E. (2003). Isotopic investigation of nitric oxide metabolism in disease. *Curr. Opin. Clin. Nutr. Metab. Care* 6, 103–108.

Lumb, A. B. (2003). Nunn's Applied Respiratory Physiology. Woburn, Butterworth-Heinemann.

Maciejewski, P. K., Kida, I., and Hyder, F. (2004). Estimating dynamic CMRO2 from dynamic CBF and BOLD fMRI

measurements. *Proc. Intl. Soc. Mag. Reson. Med.* 11, 272.

Majewska, A., Brown, E., Ross, J., and Yuste, R. (2000). Mechanisms of calcium decay kinetics in hippocampal spines: role of spine calcium pumps and calcium diffusion through the spine neck in biochemical compartmentalization. *J. Neurosci.* 20, 1722–1734.

Malinow, R., Otmakhov, N., Blum, K. I., and Lisman, J. (1994). Visualizing hippocampal synaptic function by optical detection of Ca^{2+} entry through the *N*-methyl-D-aspartate channel. *Proc. Natl. Acad. Sci. U.S.A.* 91, 8170–8174.

Mandeville, J. B., Marota, J. J., Ayata, C., Zaharchuk, G., Moskowitz, M. A., Rosen, B. R., and Weisskoff, R. M. (1999). Evidence of a cerebrovascular postarteriole Windkessel with delayed compliance. *J. Cereb. Blood Flow Metab.* 19, 679–689.

Metea, M. R., and Newman, E. A. (2007). Signalling within the neurovascular unit in the mammalian retina. *Exp. Physiol.* 92, 635–640.

Meyer, E., Müller, C. O., and Fromherz, P. (1997). Cable properties of dendrites in hippocampal neurons of the rat mapped by a voltage-sensitive dye. *Eur. J. Neurosci.* 9, 778–785.

Mintun, M. A., Vlassenko, A. G., Shulman, G. L., and Snyder, A. Z. (2002). Time-related increase of oxygen utilization in continuously activated human visual cortex. *Neuroimage* 16, 531–537.

Morikawa, E., Rosenblatt, S., and Moskowitz, M. A. (1992). L-Arginine dilates rat pial arterioles by nitric oxide-dependent mechanisms and increases blood flow during focal cerebral ischaemia. *Br. J. Pharmacol.* 107, 905–907.

Muizelaar, J. P., van der Poel, H. G., Li, Z. C., Kontos, H. A., and Levasseur, J. E. (1988). Pial arteriolar vessel diameter and CO2 reactivity during prolonged hyperventilation in the rabbit. *J. Neurosurg.* 69, 923–927.

Müller, W., and Connor, J. A. (1991). Dendritic spines as individual neuronal compartments for synaptic Ca^{2+} responses. *Nature* 354, 73–76.

Nagaoka, T., Zhao, F., Wang, P., Harel, N., Kennan, R. P., Ogawa, S., and Kim, S. G. (2006). Increases in oxygen consumption without cerebral blood volume change during visual stimulation under hypotension condition. *J. Cereb. Blood Flow Metab.* 26, 1043–1051.

Offenhauser, N., Thomsen, K., Caesar, K., and Lauritzen, M. (2005). Activity-induced tissue oxygenation changes in rat cerebellar cortex: interplay of postsynaptic activation and blood flow. *J. Physiol. (Lond.)* 565(Pt 1), 279–294.

Pasley, B. N., Inglis, B. A., and Freeman, R. D. (2007). Analysis of oxygen metabolism implies a neural origin for the negative BOLD response in human visual cortex. *Neuroimage* 36, 269–276.

Prichard, J., Rothman, D., Novotny, E., Petroff, O., Kuwabara, T., Avison, M., Howseman, A., Hanstock, C., and Shulman, R. (1991). Lactate rise detected by 1H NMR in human visual cortex during physiologic stimulation. *Proc. Natl. Acad. Sci. U.S.A.* 88, 5829–5831.

Riera, J. J., Schousboe, A., Waagepetersen, H. S., Howarth, C., and Hyder, F. (2008). The micro-architecture of the cerebral cortex: Functional neuroimaging models and metabolism. *Neuroimage* 40, 1436–1459.

Rosengarten, B., Huwendiek, O., and Kaps, M. (2001). Neurovascular coupling in terms of a control system: validation of a second-order linear system model. *Ultrasound Med. Biol.* 27, 631–635.

Royl, G., Leithner, C., Kohl, M., Lindauer, U., Dirnagl, U., Kwong, K., and Mandeville, J. (2001). The BOLD post-stimulus undershoot: fMRI versus imaging spectroscopy. *Proc. Intl. Soc. Mag. Reson. Med.* 9, 282.

Schroeter, M. L., Kupka, T., Mildner, T., Uludağ, K., and von Cramon, D. Y. (2006). Investigating the post-stimulus undershoot of the BOLD signal – a simultaneous fMRI and fNIRS study. *Neuroimage* 30, 349–358.

Schummers, J., Yu, H., and Sur, M. (2008). Tuned responses of astrocytes and their influence on hemodynamic signals in the visual cortex. *Science* 320, 1638–1643.

Schuster, A., Oishi, H., Bény, J. L., Stergiopulos, N., and Meister, J. J. (2001). Simultaneous arterial calcium dynamics and diameter measurements: application to myoendothelial communication. *Am. J. Physiol. Heart Circ. Physiol.* 280, H1088–H1096.

Seraya, I. P., and Nartsissov, Y. R. (2002). Theoretical approach to description of time-dependent nitric oxide effects in the vasculature. *Mol. Biol. Rep.* 29, 151–155.

Shen, Q., Ren, H., and Duong, T. Q. (2008). CBF, BOLD, CBV, and CMRO2 fMRI signal temporal dynamics at 500-msec resolution. *J. Magn. Reson. Imaging* 27, 599–606.

Shouval, H. Z., Bear, M. F., and Cooper, L. N. (2002). A unified model of NMDA receptor-dependent bidirectional synaptic plasticity. *Proc. Natl. Acad. Sci. U.S.A.* 99, 10831–10836.

Stefanovic, B., Schwindt, W., Hoehn, M., and Silva, A. C. (2007). Functional uncoupling of hemodynamic from neuronal response by inhibition of neuronal nitric oxide synthase. *J. Cereb. Blood Flow Metab.* 27, 741–754.

Takahashi, S., and Mendelsohn, M. E. (2003). Calmodulin-dependent and -independent activation of endothelial nitric-oxide synthase by heat shock protein 90. *J. Biol. Chem.* 278, 9339–9344.

Toda, N., and Okamura, T. (1998). Cerebral vasodilators. *Jpn. J. Pharmacol.* 76, 349–367.

Uludağ, K., Dubowitz, D. J., Yoder, E. J., Restom, K., Liu, T. T., and Buxton, R. B. (2004). Coupling of cerebral blood flow and oxygen consumption during physiological activation and deactivation measured with fMRI. *Neuroimage* 23, 148–155.

Vafaee, M. S., and Gjedde, A. (2000). Model of blood-brain transfer of oxygen explains nonlinear flow-metabolism coupling during stimulation of visual cortex. *J. Cereb. Blood Flow Metab.* 20, 747–754.

Vaughn, M. W., Kuo, L., and Liao, J. C. (1998). Effective diffusion distance of nitric oxide in the microcirculation. *Am. J. Physiol.* 274(Pt 2), H1705–H1714.

Wada, T., McKee, M. D., Steitz, S., and Giachelli, C. M. (1999). Calcification of vascular smooth muscle cell cultures: inhibition by osteopontin. *Circ. Res.* 84, 166–178.

Wang, Q., Paulson, O. B., and Lassen, N. A. (1992). Effect of nitric oxide blockade by NG-nitro-L-arginine on cerebral blood flow response to changes in carbon dioxide tension. *J. Cereb. Blood Flow Metab.* 12, 947–953.

Wang, Q., Pelligrino, D. A., Baughman, V. L., Koenig, H. M., and Albrecht, R. F. (1995). The role of neuronal nitric oxide synthase in regulation of cerebral blood flow in normocapnia and hypercapnia in rats. *J. Cereb. Blood Flow Metab.* 15, 774–778.

White, R. P., Deane, C., Vallance, P., and Markus, H. S. (1998). Nitric oxide synthase inhibition in humans reduces cerebral blood flow but not the hyperemic response to hypercapnia. *Stroke* 29, 467–472.

Wise, R. G., Pattinson, K. T., Bulte, D. P., Chiarelli, P. A., Mayhew, S. D., Balanos, G. M., O'Connor, D. F., Pragnell, T. R., Robbins, P. A., Tracey, I., and Jezzard, P. (2007). Dynamic forcing of end-tidal carbon dioxide and oxygen applied to functional magnetic resonance imaging. *J. Cereb. Blood Flow Metab.* 27, 1521–1532.

Wu, C. W., Gu, H., Lu, H., Stein, E. A., Chen, J. H., and Yang, Y. (2009). Mapping functional connectivity based on synchronized CMRO2 fluctuations during the resting state. *Neuroimage* (E-pub ahead of print).

Wu, W. C., Wang, Y., Kao, L. S., Tang, F. I., and Chai, C. Y. (2002). Nitric oxide reduces blood pressure in the nucleus tractus solitarius: a real time electrochemical study. *Brain Res. Bull.* 57, 171–177.

Yang, G., Chen, G., Ebner, T. J., and Iadecola, C. (1999). Nitric oxide is the predominant mediator of cerebellar hyperemia during somatosensory activation in rats. *Am. J. Physiol.* 277(Pt 2), R1760–R1770.

Yang, G., Zhang, Y., Ross, M. E., and Iadecola, C. (2003). Attenuation of activity-induced increases in cerebellar blood flow in mice lacking neuronal nitric oxide synthase. *Am. J. Physiol. Heart Circ. Physiol.* 285, H298–H304.

Yang, J., Clark, J. W., Bryan, R. M., and Robertson, C. S. (2005). Mathematical modeling of the nitric oxide/cGMP pathway in the vascular smooth muscle cell. *Am. J. Physiol. Heart Circ. Physiol.* 289, H886–H897.

Zappe, A. C., Uludağ, K., and Logothetis, N. K. (2008). Direct measurement of oxygen extraction with fMRI using 6% CO2 inhalation. *Magn. Reson. Imaging* 26, 961–967.

Conflict of Interest Statement: The authors declare that the research was conducted in the absence of any commercial or financial relationships that could be construed as a potential conflict of interest.

Received: 08 June 2009; paper pending published: 17 July 2009; accepted: 08 October 2009; published online: 18 November 2009.

Citation: Yücel MA, Devor A, Akın A and Boas DA (2009) The possible role of CO2 in producing a post-stimulus CBF and BOLD undershoot. Front. Neuroenerg. ***1****:7. doi: 10.3389/neuro.14.007.2009*